Materials Chemistry and Physics 141 (2013) 355–361

Contents lists available at SciVerse ScienceDirect

Materials Chemistry and Physics

journal homepage: www.elsevier.com/locate/matchemphys

Lead nitroprusside: A new precursor for the synthesis of the multiferroic $Pb_2Fe_2O_5$, an anion-deficient perovskite

Diego M. Gil [a], Gladys Nieva [b,1], Diego G. Franco [b,c], María Inés Gómez [a], Raúl E. Carbonio [c,*,1]

[a] Instituto de Química Inorgánica, Facultad de Bioquímica, Química y Farmacia, Universidad Nacional de Tucumán, Ayacucho 471, 4000 San Miguel de Tucumán, Argentina
[b] Centro Atómico Bariloche, Instituto Balseiro, Comisión Nacional de Energía Atómica, Universidad Nacional de Cuyo, 8400 San Carlos de Bariloche, Argentina
[c] Instituto de Investigaciones en Fisicoquímica de Córdoba (INFIQC – CONICET), Departamento de Fisicoquímica, Facultad de Ciencias Químicas, Universidad Nacional de Córdoba, Ciudad Universitaria, X5000HUA Córdoba, Argentina

HIGHLIGHTS

- $Pb[Fe(CN)_5NO]$ was synthesized and characterized.
- $Pb[Fe(CN)_5NO]$ belongs to orthorhombic crystal system, space group Pnma.
- $Pb_2Fe_2O_5$ was obtained by thermal decomposition of $Pb[Fe(CN)_5NO]$.
- $Pb_2Fe_2O_5$ is a weak ferromagnet due to spin canting.
- Ordering temperature of $Pb_2Fe_2O_5$ from the fit of a phenomenological model was 520 K.

GRAPHICAL ABSTRACT

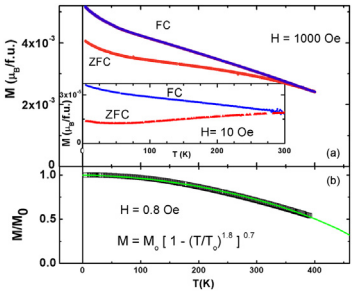

ARTICLE INFO

Article history:
Received 14 November 2012
Received in revised form
26 April 2013
Accepted 2 May 2013

Keywords:
Inorganic compounds
Magnetic materials
Powder diffraction
Thermogravimetric analysis (TGA)
Magnetic properties

ABSTRACT

In order to investigate the formation of multiferroic oxide $Pb_2Fe_2O_5$, the thermal decomposition of $Pb[Fe(CN)_5NO]$ has been studied. The complex precursor and the thermal decomposition products were characterized by IR and Raman spectroscopy, thermal analysis, powder X-ray diffraction (PXRD), scanning electron microscopy and magnetic measurements. The crystal structure of $Pb[Fe(CN)_5NO]$ was refined by Rietveld analysis. It crystallizes in the orthorhombic system, space group Pnma. The thermal decomposition in air produces highly pure $Pb_2Fe_2O_5$ as final product. This oxide is an anion deficient perovskite with an incommensurate superstructure. The magnetic measurements confirm that $Pb_2Fe_2O_5$ shows a weak ferromagnetic signal probably due to disorder in the perfect antiferromagnetic structure or spin canting. The estimated ordering temperature from the fit of a phenomenological model was 520 K. The SEM images reveal that the thermal decomposition of $Pb[Fe(CN)_5NO]$ produces $Pb_2Fe_2O_5$ with small particle size.

1. Introduction

Nitroprussides of the type $A[Fe(CN)_5NO]\cdot nH_2O$ (A = Ca, Sr, Ba) have been studied as precursors for the synthesis of perovskite type oxides $AFeO_{3-\delta}$ [1,2]. The thermal decomposition of heteronuclear complexes was demonstrated to be a promising method for the preparation of homogeneous mixed oxides at an atomic level at low

* Corresponding author. Tel.: +54 351 433 4180 ext. 127; fax: +54 351 433 4188.
E-mail addresses: carbonio@fcq.unc.edu.ar, rcarbonio@gmail.com (R.E. Carbonio).
[1] Members of the Research Career of CONICET.

0254-0584/$ – see front matter © 2013 Elsevier B.V. All rights reserved.
http://dx.doi.org/10.1016/j.matchemphys.2013.05.022

temperatures compared with the conventional ceramic method [1–7]. The use of a precursor containing the appropriate A/B ratio enforces the formation of ABO_3 perovskites with the appropriate stoichiometry, thus controlling and preventing any elements segregation generally observed in conventional methods (ceramic method) and allowing the synthesis of the desired mixed oxide at very low temperatures and with a high purity [7]. The mixed oxides obtained by this method of synthesis have relatively high surface area compared with ceramic method and could be used as catalysts in different chemical reactions [8]. On the other hand, if the ratio A/B is not appropriate like in the case of $Pb_2[Fe(CN)_6]\cdot 4H_2O$, mixtures of compounds are obtained [9,10].

Perovskite type oxides with general formula $ABO_{3-\delta}$ (A = Pb(II), Bi(III)) are considered good candidates for multiferroic materials in which ferroelectricity and magnetism coexist. This phenomena were observed in oxides such as $BiFeO_3$ [11], $BiCrO_3$ [12], $PbCrO_3$ [13] and $PbMnO_3$ [14]. The stereochemical effect of the $6s^2$ lone pair and the covalent A–O bonds (A = Pb(II) and Bi(III)) are expected to stabilize distorted non-centrosymmetric structures generating permanent electric dipoles (ferroelectricity) [13,14]. Taking these observations into account, the preparation and study of perovskite materials that have both, a cation containing lone-pair of electrons as well as a magnetic ion located at the A and/or B perovskite sites is a design strategy to obtain new multiferroic compounds. $Pb_2Fe_2O_5$, a perovskite with an incommensurate superstructure, was obtained by different methods of synthesis including ceramic method [15] or sol-gel synthesis [16]. In $Pb_2Fe_2O_5$ the co-existence of ferromagnetism and ferroelectricity has been reported [16], being in this way a good multiferroic material candidate.

In the present article we report the synthesis, structural and spectroscopic characterization of lead nitroprusside (Pb[$Fe(CN)_5NO$]) used as precursor for the synthesis of high purity $Pb_2Fe_2O_5$. The crystal structure of the complex was refined by means of Rietveld analysis using laboratory powder X-ray diffraction (PXRD). These measurements were complemented with thermogravimetric and differential thermal analysis, IR and Raman spectroscopy. The mixed oxide $Pb_2Fe_2O_5$ was obtained by thermal decomposition of the complex at 750 °C in air and it was characterized with the techniques mentioned previously. The magnetic properties of $Pb_2Fe_2O_5$ have also been investigated.

2. Experimental

2.1. Synthesis

Lead nitroprusside (PbNP) was obtained by an indirect method previously reported by different groups [1,2,17–20]. The first step corresponds to the preparation of $Ag_2[Fe(CN)_5NO]$ which was obtained by mixing aqueous solutions of $Na_2[Fe(CN)_5NO]$ and $AgNO_3$ in stoichiometric quantities under continuous stirring during two hours. The pink precipitate was separated by filtration and stored in a dry box with silica gel. In the second step, a suspension of $Ag_2[Fe(CN)_5NO]$ in water was added to a stoichiometric quantity of $PbCl_2$ aqueous solution, maintaining the mixture under vigorous stirring during 2 h. The AgCl formed was separated by filtration and the solution containing PbNP was concentrated at 60 °C. PbNP was obtained as a reddish crystalline compound, very soluble in water. The solid-state properties of the obtained material were studied with laboratory PXRD, FTIR and Raman spectroscopy and thermogravimetric and differential thermal analysis (TGA-DTA).

2.2. Characterization

TGA and DTA curves were obtained in a Shimadzu TGA/DTA-50 balance in the temperature range 20–800 °C at heating rate of 5°/min under flowing air. FTIR spectra (in the region 4000–400 cm^{-1}) were recorded at room temperature (RT) using KBr pellets, on a FTIR Perkin Elmer 1600 spectrophotometer in the transmission mode. The Raman spectrum of the solid between 3500 and 50 cm^{-1} was measured on a Thermoscientific DXR Raman microscope. Data were collected using a diode-pump, solid-state laser of 532 nm (5 cm^{-1} spectral resolution). A confocal aperture of 25 μm pinhole was used. A 10× objective was used when collecting Raman data. The sample was placed on gold-coated sample slides. In order to achieve a sufficient signal to noise ratio, 30 expositions with exposure time of 2 s were accumulated for the sample. The laser power was maintained at 10 mW when collecting data.

Laboratory PXRD profiles for PbNP and the thermal decomposition products at different temperatures were obtained at RT in a PANalytical X-Pert Pro X-ray powder diffractometer with Cu Kα radiation, between 5° and 90° in 2θ in steps of 0.02 and counting time of 1 s per step. The refinement of the crystal structure was performed by means of the Rietveld method [21] using the FULLPROF program [22].

Based in TGA results, PbNP was heated in a furnace at different temperatures in air. The sample was introduced into the furnace and heated from RT at 5°/min to the desired temperature, which was maintained for 6 h. After that, it was cooled to RT at 5°/min.

The magnetic measurements in the temperature range of 5–400 K were performed in a Quantum Design SQUID magnetometer. The magnetization values were measured after cooling in zero field (ZFC) and under an applied field (FC) for H = 0.8 Oe, 10 Oe and 1000 Oe. Magnetization vs magnetic field up to 1 T was measured at several fixed temperatures.

3. Results and discussion

3.1. Pb[Fe(CN)$_5$NO]

3.1.1. Crystal structure refinement

The PXRD pattern of PbNP refined at RT is shown in Fig. 1. Final cell parameters, atomic positions and discrepancy factors are shown in Table 1. Fig. 2 shows the atomic packing within the unit cell and the coordination environment for Pb and Fe atoms. Anhydrous PbNP crystallizes in the orthorhombic crystal system, in the space group Pnma. In the crystal structure the iron atom is coordinated to five C atoms of CN ligands and to the N atom of the NO group. The resulting octahedron, $[Fe(CN)_5NO]^{2-}$, is distorted due to the larger electron withdrawing effect (π-back bonding) of the NO group with respect to the cyanide ligand. PbNP is isostructural with the complexes M[$Fe(CN)_5NO$] (M = Mn, Zn, Cd) were the outer metal cation (Mn, Zn or Cd) is coordinated by five CN

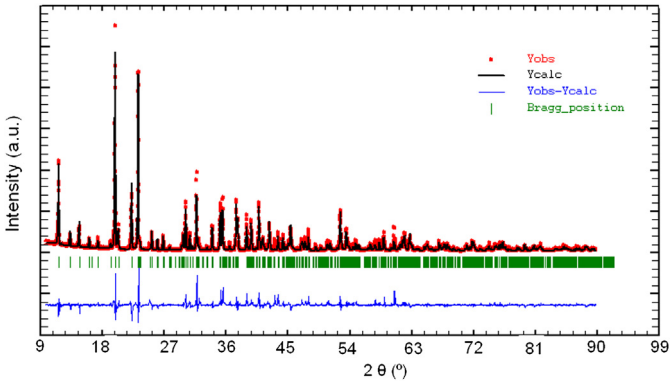

Fig. 1. PXRD pattern observed (red), calculated (black) and difference curve (blue) for the Rietveld refinement of Pb[$Fe(CN)_5NO$]. (For interpretation of the references to color in this figure legend, the reader is referred to the web version of this article.)

Table 1
Crystallographic parameters and discrepancy factors for $Pb[Fe(CN)_5NO]$ after Rietveld refinement with PXRD data obtained at RT.

Atom	Wyckoff site	*x*	*y*	*z*
Pb	4c	0.0076 (1)	0.75	0.3581 (1)
Fe	4c	0.2834 (4)	0.25	0.3546 (6)
N1	4c	0.2288 (4)	0.25	0.1883 (4)
O	4c	0.1839 (3)	0.25	0.0889 (3)
C1	4c	0.3661 (5)	0.25	0.5498 (5)
C2	8d	0.1972 (3)	0.0734 (5)	0.4010 (3)
C3	8d	0.3742 (3)	0.0829 (5)	0.3263 (4)
N2	4c	0.3393 (3)	0.25	0.6475 (4)
N3	8d	0.1571 (2)	0.0018	0.4721 (3)
N4	8d	0.4343 (2)	0.0047	0.3257 (3)

Space group: Pnma; cell parameters: $a = 13.2658$ (2) Å, $b = 7.9791$ (1) Å, $c = 9.2366$ (1) Å, $V = 977.71$ (3) Å^3; $Z = 4$.
Discrepancy factors: $R_{wp} = 23.5$; $R_{exp} = 7.93$; $\chi^2 = 8.76$; $R_B = 10.98$; $R_p = 20.2$.

ligands [23]. The most interesting characteristic of this structure is the penta-fold coordination of Pb(II) ions (Fig. 2). The coordination polyhedron of Pb (a distorted square pyramid) is formed by five N atoms from CN ligands. This type of coordination was observed in $Pb_2[Fe(CN)_6]\cdot 4H_2O$ where Pb(II) can not stabilize an octahedral coordination due to its low polarizing power [10] and because the sixth position of the octahedron is occupied by the sp hybridized lone pair of Pb(II). The irregular octahedra and the distorted square pyramid are bridged through CN groups.

3.1.2. Vibrational study

Fig. 3(a) shows the FTIR spectrum in the region of 4000–400 cm^{-1} at RT in KBr disks. The inset shows the expanded region where the stretching bands of isolated CN and NO groups appear (see below). Raman spectrum measured at room temperature is shown in Fig. 3(b). Table 2 collects Infrared and Raman wavenumbers and their tentative assignments. The assignments of the bands corresponding to the nitroprusside ion were performed by comparison with the spectra of other nitroprussides previously studied [17–20].

3.1.2.1. CN stretching bands. Six bands are observed in the IR spectrum in the 2300–1850 cm^{-1} range (inset Fig. 3a). The band located at 2180 cm^{-1} in the IR and Raman spectra is assigned to CN groups in axial positions and the bands located at 2164, 2157 and 2142 cm^{-1} are assigned to equatorial CN groups. This assignment was performed considering the C_{4v} symmetry of the nitroprusside anion (one axial and three equatorial CN stretching modes). The weak bands observed at 2110 and 2097 cm^{-1} are assigned to $^{13}C^{14}N$ stretching modes due to the presence of ^{13}C in relative natural abundance. It is assumed that the bands due to the $^{13}C^{15}N$ species are too weak to be observed in IR and Raman spectra.

3.1.2.2. NO and FeNO vibrational bands. The bands located at 1951 and 1938 cm^{-1} could be assigned to the $^{14}N^{16}O$ stretching typical of the nitroprusside ions. The very weak band observed at 1903 cm^{-1} could be assigned to any of the isotopic NO groups; in this case we assume that the isotopic group present in this compound is $^{15}N^{16}O$ (0.38% of abundance) [17,18]. In agreement with the very low Raman intensity of the NO stretching, no Raman band was observed for this group in PbNP. In the region comprised between 1500 and 700 cm^{-1}, bands due to the first overtones of δ(FeNO) and ν(FeN) and to combinations of fundamental bands are present. Second overtones are surely overlapped by the strong νNO fundamental band.

The bands at 661 and 638 cm^{-1} are assigned to the FeNO bending and FeN stretching modes, respectively [17–20].

3.1.2.3. FeC stretching and FeCN bandings. The band at 503 cm^{-1} in the IR spectrum could be assigned to a combination of CFeC bending and FeC stretching modes. The band located at 468 cm^{-1} is assigned to a combination of two modes, ν(FeN) and δ(FeCN) and

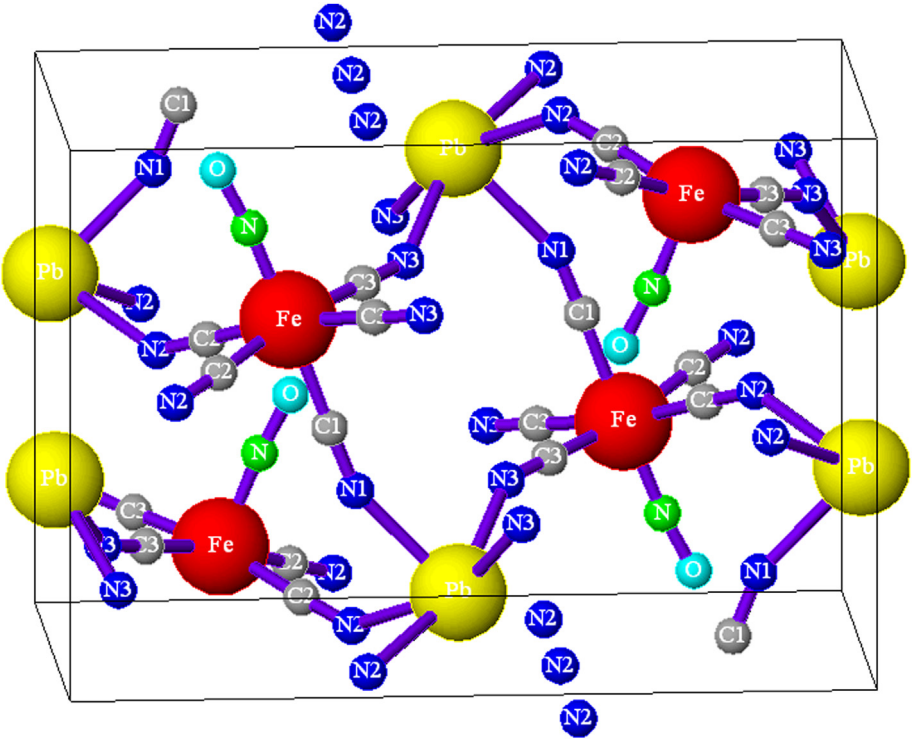

Fig. 2. Crystal packing within the unit cell and coordination environment for Fe(II) and Pb(II) in $Pb[Fe(CN)_5NO]$.

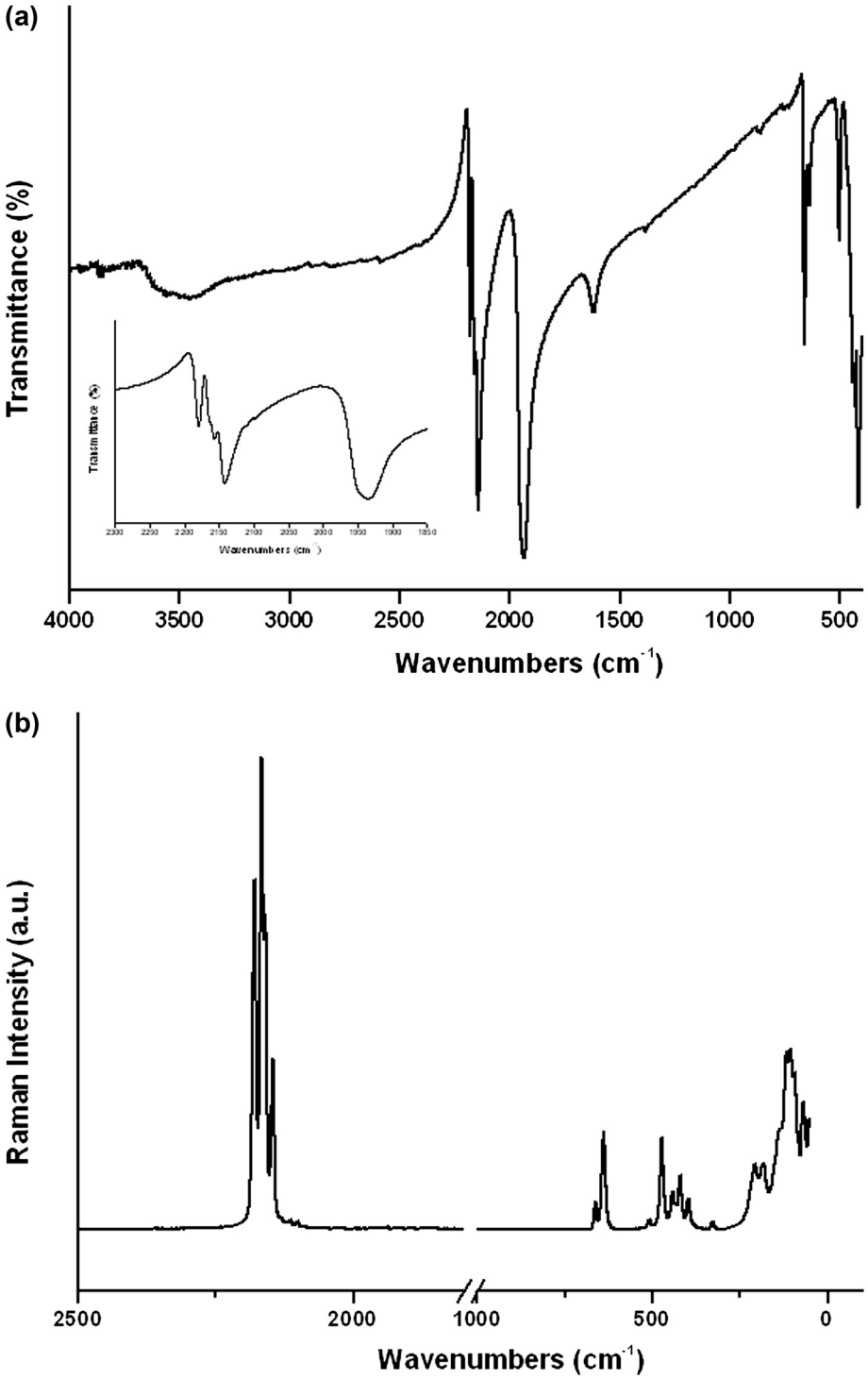

Fig. 3. (a) Infrared spectra of $Pb[Fe(CN)_5NO]$ in the 4000–400 cm^{-1} at room temperature. Inset: IR spectrum between 2300 and 2850 cm^{-1}. (b) Raman spectrum of $Pb[Fe(CN)_5NO]$ at room temperature.

the bands at 431 and 418 cm^{-1} are attributed to FeC stretching modes. The band located at 398 cm^{-1} has appreciable intensity in the Raman spectrum, suggesting that it can be assigned to FeC_{eq} stretching mode. In the region 200–50 cm^{-1} appear $NFeC_{eq}$, C_{eq}-FeC_{eq} and $C_{ax}FeC_{eq}$ bending bands and lattice modes. In this region the Raman spectra are more helpful than the infrared spectra due to the higher intensity and better definition of bands. See Table 2 for IR and Raman wavenumbers and assignments.

3.1.3. Thermal decomposition

The thermal behavior of the complex PbNP was studied by TG and DT analysis. Fig. 4(a) and (b) shows TG and DTA curves, respectively for the thermal decomposition of lead nitroprusside in air. Only one step for the thermal decomposition of PbNP is observed in TG curve. The decomposition step starts at 222 °C and finishes at approximately 482 °C. This step was associated to the simultaneous elimination and oxidation of CN and NO groups.

Table 2
Observed Infrared and Raman wavenumbers (cm^{-1}) with assignments for Pb $[Fe(CN)_5NO]$ at room temperature.

Infrared	Raman	Assignment
2180	2180	ν(CN) axial
2164	2166	ν(CN) equatorial
2157	2160	ν(CN) equatorial
2142	2146	ν(CN) equatorial
2110	2114	$\nu(^{13}C^{14}N)$
2097	2100	$\nu(^{13}C^{14}N)$
1951	–	$\nu(^{14}N^{16}O)$
1938	–	$\nu(^{14}N^{16}O)$
1903	–	$\nu(^{15}N^{16}O)$
661	662	δ(FeNO)
638	638	ν(FeN)
503	508	$\delta(C_{ax}FeC_{eq}) + \nu(FeC_{eq})$
468	472	ν(FeN) + $\delta(FeCN_{eq})$
442	443	$\delta(FeCN_{eq})$
431	432	$\delta(FeCN_{ax})$
418	420	$\nu(FeC_{eq})$
–	398	$\nu(FeC_{eq})$
–	383	$\nu(FeC_{ax})$
–	327	$\delta(FeCN_{eq})$
–	207	?
–	184	?
–	136	?
–	117	$\delta(NFeC_{eq}) + \delta(C_{ax}FeC_{eq})$
–	105	$\delta(C_{eq}FeC_{eq})$
–	94	$\delta(NFeC_{eq})$
–	69	$\delta(NFeC_{eq})$
–	53	?

Amalvy et al. have reported that the thermal decomposition of potassium nitroprusside involves two steps for the elimination of NO and CN ligands. The first step is associated to the elimination of NO ligand and the second one involves the elimination of CN groups [17]. This behavior was observed in alkaline and alkaline earth nitroprussides [1,2,17–20]. The total mass loss observed was 28.11 % and it was in agreement with the theoretical value (28.36%) calculated for the formation of $Pb_2Fe_2O_5$ from PbNP.

The DTA curve shows an exothermic peak located at 372 °C and it corresponds to the elimination and oxidation (combustion) of the NO and cyanide groups.

3.2. Characterization of products of thermal treatments of Pb $[Fe(CN)_5NO]$

3.2.1. PXRD

In order to analyze the oxides obtained after thermal decomposition of lead nitroprusside in air atmosphere at different temperatures, the resulting products at each step were characterized by laboratory PXRD (Fig. 5). The composition of the residues at different temperatures was determined using the X'Pert Highscore Program (version 2.1b, PANalytical, B.V. Almelo, The Netherlands). When the complex was heated at 400 and 450 °C, some peaks attributed to Fe_2O_3 (PDF # 049-1139), Fe_3O_4 (PDF # 089-6466), PbO massicot (PDF # 085-1739) and PbO litharge (PDF # 005-0570) were observed, showing an incomplete reaction. When the complex was heated at 550 °C, the peaks corresponding to PbO (massicot and litharge) were observed together with some peaks attributed to $Pb_2Fe_2O_5$ (PDF # 033-0756). When the complex was heated at 750 °C, the PXRD shows only lines corresponding to $Pb_2Fe_2O_5$. The JCPD card assigns a tetragonal structure to $Pb_2Fe_2O_5$. However, Abakumov et al. have reported this oxide with a monoclinic structure by analysis of HRTEM images and electron diffraction patterns [15]. Recently, Batuk et al. have solved the crystal structure of $Pb_2Fe_2O_5$ from transmission electron microscopy data [24]. $Pb_2Fe_2O_5$ with an incommensurate superstructure crystallizes

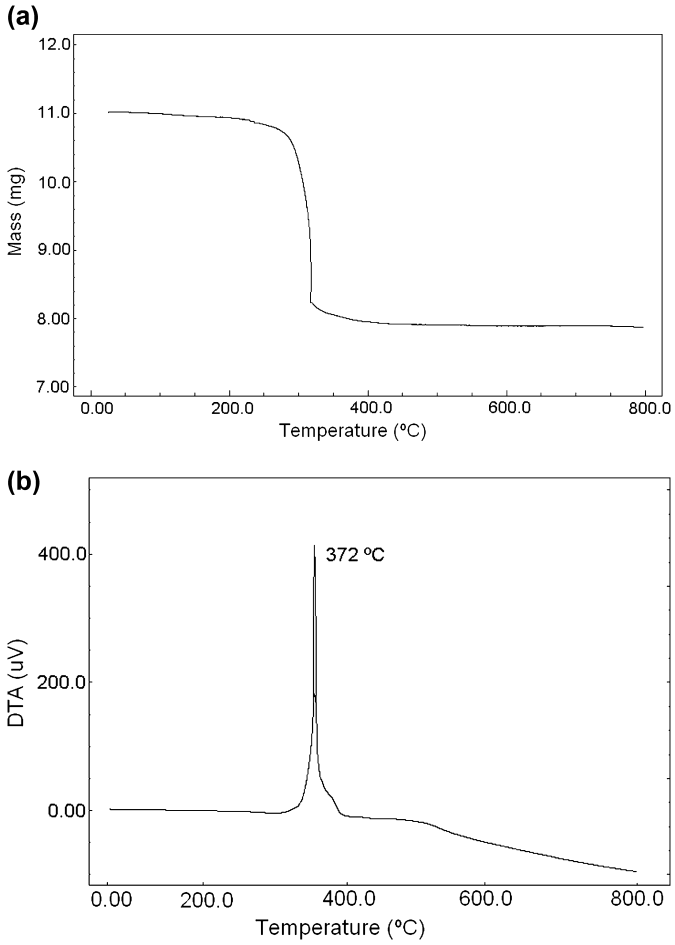

Fig. 4. (a) TGA curve for Pb$[Fe(CN)_5NO]$ in air. (b) DTA curve for Pb$[Fe(CN)_5NO]$ in air.

in a tetragonal system, in the space group I4/mmm. The structure can be represented as an intergrowth of perovskite blocks and partially disordered blocks with a structure similar to that of the Bi_2O_2 blocks in Aurivillius-type phases. The layered $Pb_2Fe_2O_5$ is

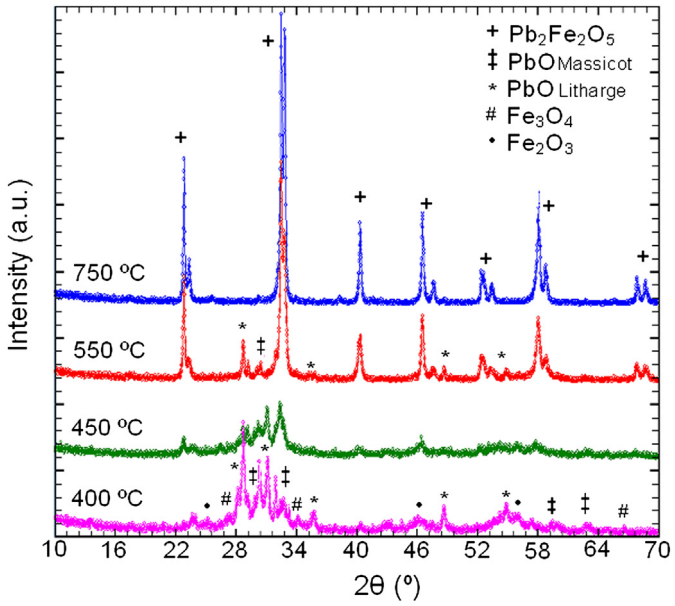

Fig. 5. PXRD data of samples obtained by thermal decomposition of Pb$[Fe(CN)_5NO]$ at 400, 450, 550 and 750 °C.

expected to be an anion-deficient perovskite and it adopts a crystallographic shear planes structure with alternating layers of FeO_5 pyramids and FeO_6 octahedra [15,24].

3.2.2. FTIR

The FTIR spectra of the samples obtained by thermal decomposition of PbNP at 550 and 750 °C are shown in Fig. 6. Both spectra are very similar and present a very simple spectral pattern, as usually found in perovskite materials [1,2,5–7,10]. The spectra show two groups of bands, together with a certain number of weak shoulders due to the low symmetry of this compound. The very strong bands at around 550 and 530 cm^{-1} are split in three components at 546, 536 and 530 cm^{-1} and it could be assigned to the antisymmetric stretching vibration of the FeO_6 octahedra. The splitting observed in the IR bands of this compound could be attributed to the distortion caused by the $6s^2$ lone pair of the Pb(II) cation. The bands located at 418 cm^{-1} can be assigned to the antisymmetric deformation of the FeO_6 octahedra. The bands at 487 cm^{-1} could be attributed to Pb–O stretching vibration.

3.2.3. Magnetic properties

Fig. 7(a) shows the temperature dependence of the magnetization (M) under both ZFC (zero field cooling) and FC (field cooling) conditions, at 10 Oe and 1000 Oe, for $Pb_2Fe_2O_5$ obtained at 750 °C. An important difference between both curves is observed in the whole temperature range, which is a clear indication of a ferromagnetic interaction in $Pb_2Fe_2O_5$. The Néel temperature was not observed because it exceeded the temperature range of the equipment. T_N determined by Grenier et al. was 555 K [25].

Fig. 7(b) shows the remnant magnetization vs Temperature data taken at low applied field, $H = 0.8$ Oe, after magnetizing the sample at 1 T. The sample was cooled in this very low field from 400 K to 5 K and the remnant magnetization was used to estimate the ordering temperature using a phenomenological model [26] (see expression in Fig. 7(b)) that combine the behaviors at the two limits $T \sim 0$ K and $T \sim T_c$. The estimated ordering temperature from the fit was 520 K. This ordering temperature, which is lower than the T_N determined by Grenier et al. [25], could be related with an antiferromagnetic bulk ordering occurring at this temperature that yield the small ferrimagnetic signal that we observed.

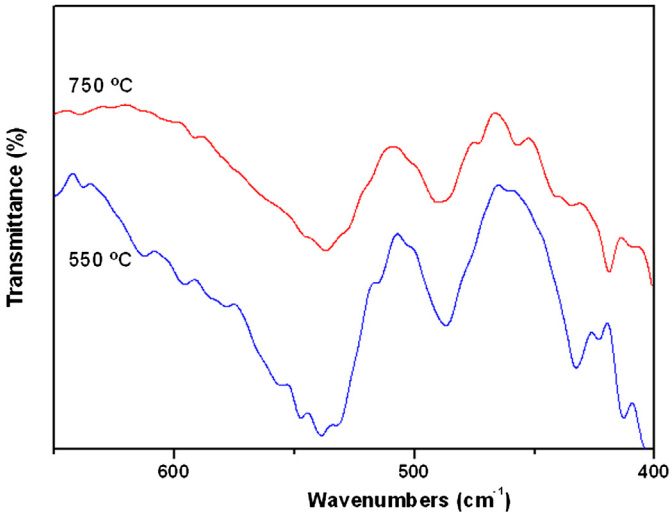

Fig. 6. IR spectra for the samples obtained by thermal decomposition of Pb $[Fe(CN)_5NO]$ at 550 and 750 °C.

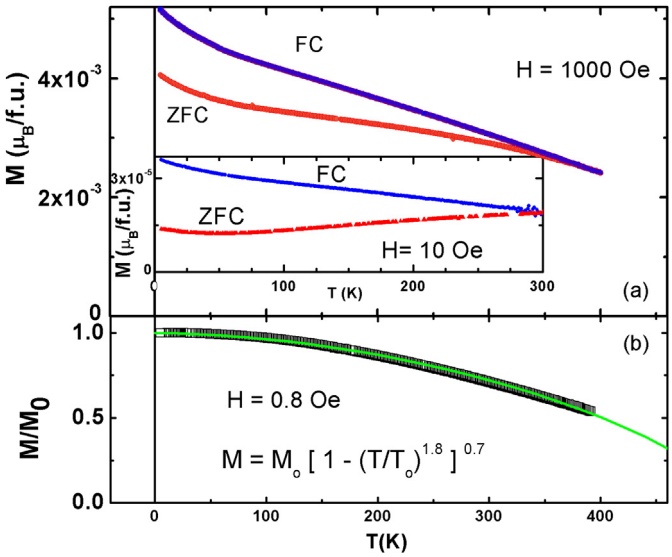

Fig. 7. (a) Field cooling (FC) and zero field cooling (ZFC) magnetization curves at $H = 10$ and 1000 Oe for $Pb_2Fe_2O_5$ obtained at 750 °C. (b) Remnant magnetization after applying $H = 1$ T, FC procedure at 0.8 Oe. The fitted expression (see text) yield an ordering temperature $T_o = 520$ K.

Magnetization versus magnetic field (H) measurements at 400 K, 50 K and 5 K are shown in Fig. 8. A characteristic hysteresis cycle with a weak ferromagnetic signal is obtained, the upper inset shows the ferromagnetic signal subtracted from a linear background in the M vs H curve. At 5K, a saturation moment of $\sim 9.5 \times 10^{-3}$ μ_B/f.u. could be depicted with a remnant moment as low as 3×10^{-3} μ_B/f.u. The coercive field vs temperature is shown in the lower inset of Fig. 8, our values are in agreement with those reported by Wang et al. [16] (1700 Oe). The value of the saturated moment of the ferromagnetic signal is very small, about 10^{-3} times the one expected for saturated Fe(III) moments. This could be due to the alignment of ordered Fe(III) moments being not strictly antiparalell but slightly canted, this results in a small net magnetization, giving rise a weak ferromagnetic behavior [13]. Also a small amount of disorder could hinder the perfect antiferromagnetic ordering resulting in the small ferromagnetic signal that we observed.

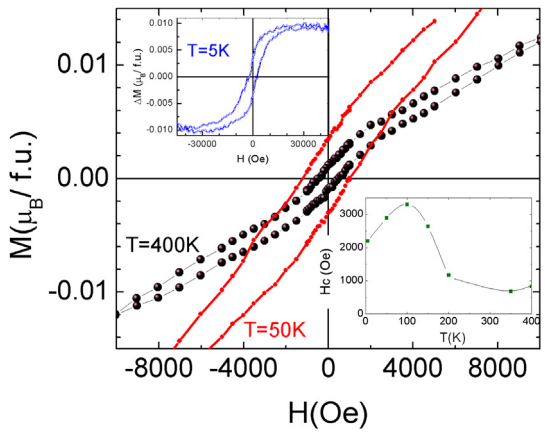

Fig. 8. Hysteresis loops at 400 K and 50 K raw data for $Pb_2Fe_2O_5$ sample obtained at 750 °C. The upper inset shows the ferromagnetic contribution at 5 K. ΔM was obtained subtracting a linear term to the M vs H data. The lower inset shows the coercive field extracted from the hysteresis loops after subtracting the high field linear contribution.

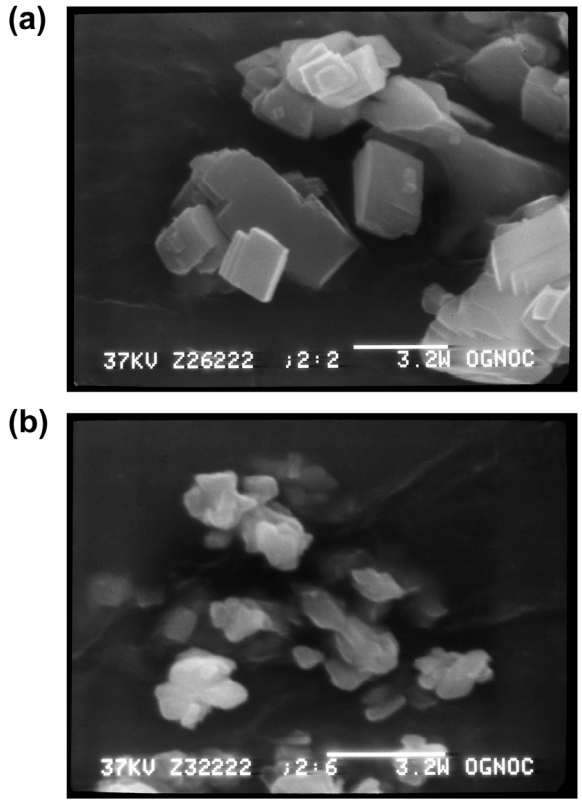

Fig. 9. Scanning electron microscopy of (a) $Pb[Fe(CN)_5NO]$ and (b) $Pb_2Fe_2O_5$ obtained at 750 °C.

3.2.4. Scanning electron microscopy

The size and morphologies of PbNP and its thermal decomposition products were investigated by SEM (Fig. 9). The SEM photograph of $Pb[Fe(CN)_5NO]$ powder shows that it is composed of well defined crystals with plate shapes and around 3 μm size. The SEM photograph of $Pb_2Fe_2O_5$ obtained for samples synthesized at 750 °C clearly shows that the shape and morphology are quite different to the one of its precursor complex. The crystals of the precursor were disrupted by the evolving gases and fine particles of the order of 1.5 μm appeared.

4. Conclusions

In this study, highly pure $Pb_2Fe_2O_5$ was synthesized by thermal decomposition of $Pb[Fe(CN)_5NO]$ (PbNP). PbNP decomposes in one step by losing the CN and NO groups to produce $Pb_2Fe_2O_5$ as final product.

The crystal structure of PbNP was refined from PXRD data using Rietveld analysis. This compound crystallizes in the orthorhombic system, space group Pnma and $Z = 4$. In this structure the Fe atoms are octahedrally coordinated to five CN ligands and a NO group and Pb(II) cations are penta-fold coordinated to five N atoms from CN ligands. In this complex, Pb(II) cations can not stabilize an octahedral coordination due to its low polarizing power and the s^2 lone pair hybridized sp.

The vibrational behavior of PbNP was analyzed using IR and Raman spectroscopy. The complete bands assignment was performed in comparison with related nitroprussides.

$Pb_2Fe_2O_5$ was obtained as a pure phase by thermal decomposition of PbNP at 750 °C in air and it adopts an incommensurate structure with crystallographic share planes. It crystallizes in the tetragonal system, space group I4/mmm. The SEM images reveal that the thermal decomposition of PbNP produces $Pb_2Fe_2O_5$ with small particle size.

According to the magnetic measurements, $Pb_2Fe_2O_5$ shows a weak ferromagnetic behavior that could be due to spin canting or disorder in the perfect antiferromagnetic structure. The estimated ordering temperature from the fit of a phenomenological model using the remnant magnetization was 520 K.

Acknowledgments

R.E.C. thanks FONCYT for PICT2007 303, CONICET for PIP #11220090100995 and SECyT-UNC for the Project 162/12. D.M.G. and D.G.F. thank CONICET for a fellowship. D.M.G. and M.I.G. thank CIUNT for financial support, Project 26D-428. G.N. thanks FONCYT for PICT2007 819, CONICET for PIP #11220090100448 and SECTyP-UNCuyo.

References

[1] M.I. Gómez, J.A. de Moran, R.E. Carbonio, P.J. Aymonino, J. Solid State Chem. 142 (1999) 138–145.
[2] M.I. Gómez, G. Lucotti, J.A. de Moran, P.J. Aymonino, S. Pagola, P. Stephens, R.E. Carbonio, J. Solid State Chem. 160 (2001) 17–24.
[3] P.K. Gallagher, Mater. Res. Bull. 3 (1968) 225–232.
[4] E. Traversa, P. Nunziante, M. Sakamoto, Y. Sadaoka, M.C. Carotta, G. Martinelli, J. Mater. Res. 13 (1998) 133–134.
[5] M.C. Navarro, E.V. Pannunzio Miner, S. Pagola, M.I. Gómez, R.E. Carbonio, J. Solid State Chem. 178 (2005) 847–854.
[6] M.C. Navarro, M.C. Lagarrigue, J.M. de Paoli, R.E. Carbonio, M.I. Gómez, J. Therm. Anal. Calorim. 102 (2010) 655–660.
[7] D.M. Gil, M.C. Navarro, M.C. Lagarrigue, J. Guimpel, R.E. Carbonio, M.I. Gómez, J. Therm. Anal. Calorim. 103 (2011) 889–896.
[8] Y. Itagaki, M. Mori, Y. Hosoya, H. Aono, Y. Sadaoka, Sens. Actuators B 122 (2007) 315–320.
[9] D.M. Gil, R.E. Carbonio, M.I. Gómez, J. Chil. Chem. Soc. 55 (2010) 189–192.
[10] D.M. Gil, M. Avila, E. Reguera, S. Pagola, M.I. Gómez, R.E. Carbonio, Polyhedron 33 (2012) 450–455.
[11] K.Y. Yun, M. Noda, M. Okuyama, J. Appl. Phys. 96 (2004) 3399–3403.
[12] A.A. Belik, N. Tsujii, H. Suzuki, E. Takayama-Muromachi, Inorg. Chem. 46 (2007) 8746–8751.
[13] A.M. Arévalo-López, A.J. Dos Santos García, M.A. Alario-Franco, Inorg. Chem. 48 (2009) 5434–5438.
[14] K. Oka, M. Azuma, S. Hirai, A.A. Belik, H. Kojitani, M. Akaogi, M. Takano, Y. Shimakawa, Inorg. Chem. 48 (2009) 2285–2288.
[15] A.M. Abakumov, J. Hadermann, S. Bals, I.V. Nikolaev, E.V. Antipov, G. Van Tendeloo, Angew. Chem. Int. Ed. 45 (2006) 6697–6700.
[16] M. Wang, G. Tang, Mater. Res. Bull. 46 (2011) 438–441.
[17] J. Amalvy, E.L. Varetti, P.J. Aymonino, J. Phys. Chem. Solids 46 (1985) 1153–1161.
[18] J. Amalvy, E.L. Varetti, P.J. Aymonino, J. Crystallogr. Spectrosc. Res. 16 (1986) 537–555.
[19] M.M. Vergara, E.L. Varetti, Spectrochim. Acta 49 (1993) 527–534.
[20] C.O. Della Vedova, J.H. Lesk, E.L. Varetti, P.J. Aymonino, J. Mol. Struct. 70 (1981) 241–254.
[21] R.A. Young, The Rietveld Method, Oxford Scientifics Publications, UK, 1995.
[22] J. Rodriguez-Carbajal, Physica B 192 (1993) 55–69.
[23] J. Rodríguez-Hernandez, E. Reguera, M. Mir, Y.P. Mascarenhas, Powder Diffrac. 22 (2007) 40–46.
[24] D. Batuk, J. Hadermann, A.M. Abakumov, T. Vranken, A. Hardy, M.V. Bael, G.V. Tendeloo, Inorg. Chem. 50 (2011) 4978–4986.
[25] J. Grenier, M. Pouchard, P. Hagenmuller, Rev. Chim. Miner. 14 (1977) 515–522.
[26] (a) I.V. Nikolaev, H. D'Hondt, A.M. Abakumov, J. Hadermann, A.M. Balagurov, I.A. Bobrikov, D.V. Sheptyakov, V.Yu. Pomjakushin, K.V. Pokholok, D.S. Filimonov, G. Van Tendeloo, E.V. Antipov, Phys. Rev. B 78 (2008) 024426; (b) O.E. Korneychik, M. Batuk, A.M. Abakumov, J. Hadermann, M.G. Rozova, D.V. Sheptyakov, K.V. Pokholok, D.S. Filimonov, E.V. Antipov, J. Solid State Chem. 184(2011) 3150–3157.